Title: Photochemical production of sulfate and methanesulfonic acid from dissolved organic sulfur

Authors: Rachele Ossola[1], Julie Tolu[1,2], Baptiste Clerc[1], Paul R. Erickson[1], Lenny H. E. Winkel[1,2], Kristopher McNeill[1,*]

Affiliations

[1] Institute of Biogeochemistry and Pollutant Dynamics (IBP), Department of Environmental System Science, ETH Zürich, 8092 Zürich Switzerland

[2] Eawag Swiss Federal Institute of Aquatic Science and Technology, 8600 Dübendorf Switzerland

*Correspondence to: kristopher.mcneill@env.ethz.ch

Abstract

Despite its importance in biological processes and its influence on metal bioavailability, the biogeochemical cycle of dissolved organic sulfur (DOS) in aquatic systems is still poorly understood. Recent high-resolution mass spectrometry (HRMS) studies showed a selective loss of organic sulfur during photodegradation of dissolved organic matter (DOM), which was hypothesized to result in the production of sulfate. Here, we provide evidence of ubiquitous production of sulfate, methanesulfonic acid (MSA) and methanesulfinic acid (MSIA) during photodegradation of DOM samples from a wide range of natural terrestrial environments. We show that photochemical production of sulfate is generally at least one order of magnitude more efficient than the production of MSA and MSIA, as well as volatile S-containing compounds (*i.e.*, CS_2 and COS). We also identify possible molecular precursors for sulfate and MSA, and we demonstrate that a wide range of relevant classes of DOS compounds (in terms of S oxidation state

and molecular structure) can liberate sulfate upon photosensitized degradation. This work indicates that photochemistry plays a more significant role in the aquatic and atmospheric cycle of DOS than currently believed.

Main Text

Dissolved organic sulfur (DOS) can be defined as the fraction of dissolved organic matter (DOM) composed of molecules that contain at least one sulfur atom. Dimethylsulfide (DMS), a volatile biogenic compound found in marine surface waters, is one of the DOS compounds that has so far received the most attention due to its role in climate regulation.[1–3] Ksionzek *et al.* recently pointed out that DMS and other known and studied DOS compounds such as dimethylsulfoniopropionate (DMSP), carbonyl sulfide (COS) and carbon disulfide (CS_2), represent only a small fraction (≈ 0.35%) of the total oceanic DOS pool.[4] The same study also reported evidence of a rapid turnover, *i.e.* production and remineralization, of biologically derived DOS occurring in the surface mixed layer, in contrast with the refractory character of DOS present deeper in the water column.[4] Despite these new findings, many questions remain unresolved on the biogeochemical cycle of DOS. The lack of knowledge is even more striking for freshwater environments, which have received very little attention despite their higher DOS levels compared to the marine systems.

In recent years, photochemistry has been recognized as a potential driver in the DOS cycle. Studies using high-resolution mass spectrometry (HRMS) showed a high photochemical reactivity of sulfur-containing organic molecules from saltmarsh,[5] deep sea[6] and acid mine drainage[7]. These studies consistently reported faster degradation kinetics of CHOS formulas compared to CHO formulas and observed the conversion of CHOS into CHO, implying photochemical loss of organic sulfur. Based on mass balance considerations, we hypothesized that the loss of sulfur should be associated with the formation of sulfate (photomineralization) and/or other small oxidized S-

containing molecules that might elude HRMS detection. This hypothesis is supported by the available literature on the photochemistry of DMS, COS and CS_2[8,9] and has already been put forward by some authors[6,7]. In this work, we provide experimental support for this hypothesis by demonstrating that non-volatile DOS undergoes facile photochemical conversion to sulfate and other small non-volatile compounds, such as methanesulfonic acid (CH_3SO_3H, MSA) and methanesulfinic acid (CH_3SO_2H, MSIA), under environmentally relevant conditions.

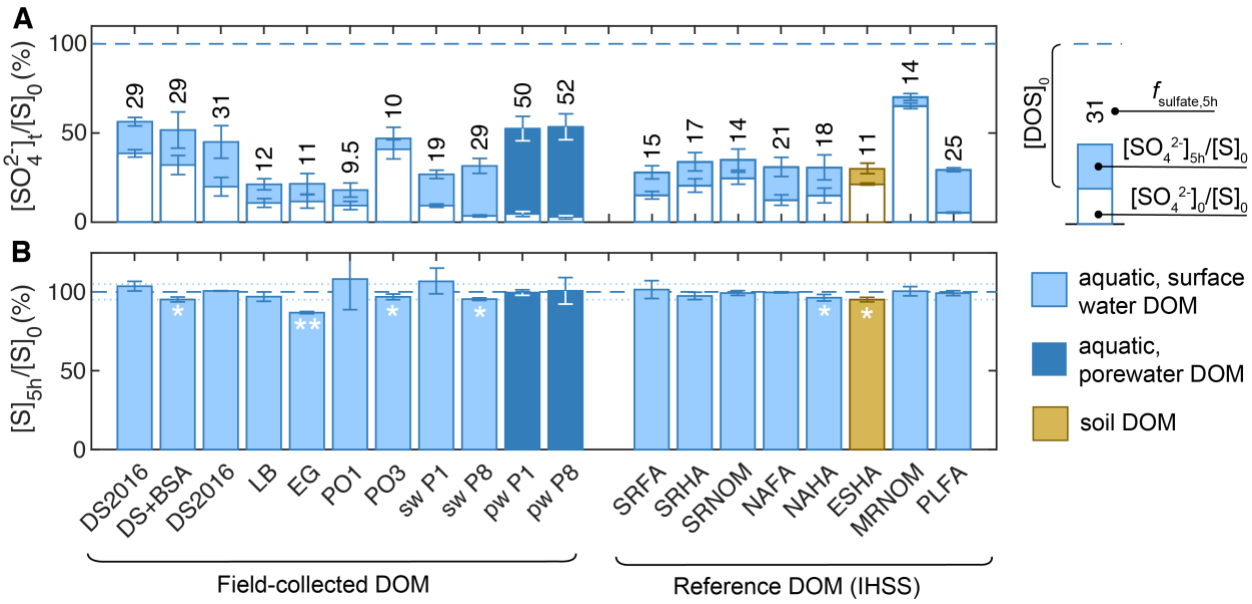

Figure 1 Photochemically induced changes in sulfur speciation in reference and field-collected DOM samples. A. White and blue bars represent $[S]_0$-normalized sulfate concentrations at the beginning and at the end of the irradiation, respectively. The numbers above the bars indicate the fraction of $[DOS]_0$ converted to sulfate after 5 hours of UVB irradiation ($f_{sulfate,5h}$). The error bars are obtained from error propagation of the standard deviations in $[S]_0$, $[SO_4^{2-}]_0$ and $[SO_4^{2-}]_{5h}$ (triplicate measurements). In these experiments, 5 hours of irradiation were approximately equivalent to 11 hours during a clear midsummer day (Supplementary Text S4; $I = 64 \pm 4$ J s^{-1} m^{-2}). **B.** Changes in total sulfur during UVB irradiation experiments. The error bars are standard deviations of independent triplicate experiments, while the asterisk(s) indicates samples with $[S]_{5h}/[S]_0$ (± error) below unity (* = value within 5%; ** = value within 10%). In these experiments, the absolute irradiance was 45 ± 4 J s^{-1} m^{-2} ($\Delta\lambda$ = 290 – 400 nm). The acronyms for the waters can be found in Table S5, while the numeric values of $f_{photo,5h}$ and $[S]_{5h}/[S]_0$ and their associated experimental errors are in Table S1.

Photochemical production of sulfate from DOS

Aqueous solutions of reference DOM isolates from soil, river and lakes and field-collected natural waters from lakes, swamps and peat bogs were irradiated with UVB light under laboratory conditions, and sulfate photoproduction was quantified via ion chromatography (Figure S1). This collection of materials was chosen to reflect a wide range of natural DOM variability, from terrestrially- (*i.e.*, Dismal Swamp; DS) to microbially-derived (*i.e.*, Pony Lake fulvic acid; PLFA) organic matter end members.[10,11]

Overall, 10 to 50% of the initial DOS was mineralized to sulfate after an irradiation approximately equivalent to a whole clear midsummer day ($f_{sulfate,5h}$, Figure 1A), even though variations were observed across samples. Significantly higher $f_{sulfate,5h}$ were obtained for the Prairie Pothole porewaters (50 ± 5 % and 52 ± 4 %) compared to the surface waters of the corresponding pools (19 ± 1 % and 29 ± 4 %, respectively), which exhibited photochemical behavior analogous to the other field-collected surface waters and the reference DOM samples ($f_{sulfate,5h} \approx 10 - 30\%$). Smaller variations could also be identified within the surface water samples. For instance, $f_{sulfate,5h}$ values of the Prairie Pothole surface waters, the three DS samples and PLFA were overall higher than the other samples (27 ± 4 % (N = 6) *vs* 14 ± 3 % (N = 11)), even though they were not statistically different as judged by a 2-tailed t-test (P = 0.69). These differences can be tentatively rationalized by specific characteristics of these three environments. Sleighter *et al.* showed that diagenetic sulfurization occurs in the Prairie Pothole sediments, resulting in the formation of an abundant pool of S-enriched DOM that is not found in typical lacustrine environments,[12] as confirmed by the low DOC/DOS ratios of the porewaters compared to the other samples (Table S1). Water circulation within the wetland brings the S-enriched DOS from the sediments to the surface,[12,13] where oxidative transformations can occur.[5,13] Thus, the Prairie Pothole surface waters are

expected to be more reactive than common surface waters due to a higher content of organic sulfur, but less reactive than the corresponding porewaters due to a lower fraction of reduced sulfur species. Dismal Swamp is characterized by a relatively high iron content and high hydroxyl radical steady-state concentrations (during irradiation),[14] which may trigger DOS degradation mechanisms that would otherwise be of limited relevance. Finally, the higher photochemical reactivity of PLFA might be related to its molecular composition, which is dominated by bacterial- and algal-derived organic matter.[10] This difference in source material compared to terrestrially derived DOM might result in a different distribution of S oxidation states, an increased photochemical reactivity (already documented for triplet DOM-related processes)[15], or a combination of these two factors.

To test whether complete photomineralization occurs, long-term irradiations were also performed on PLFA and DS water (Figure 2A and S3A). Both samples showed a clear plateau in sulfate production, with a fractional yield ($Y_{sulfate}$; *vide infra*) of 67% and 85% for PLFA and DS, respectively. This result implies that the majority, but not all, of $[DOS]_0$ could be converted to sulfate, suggesting that photorefractory (*i.e.*, photochemically stable) compounds might be present before or might be formed during irradiation. Furthermore, in PLFA, the plateau was observed when sulfate production was plotted *vs* absorbed photons (Figure 2A), while in DS the plateau was observed when using irradiation time as x-axis (Figure S3A). The difference between irradiation time and absorbed photons is related to photobleaching, *i.e.*, the destruction of chromophores, which is a well-known process in DOM photochemistry.[16] This phenomenon was observed for both waters (Figure S3B), but appeared relevant for PLFA only, hinting that different sulfate production mechanisms might be active in the two samples.

For more insight into the sulfate production mechanisms, we analyzed the sulfate photoproduction kinetics and tested for correlations with relevant water chemistry parameters. We fitted the sulfate concentration profiles with an exponential growth function (equation (1); Figure S1), where the pre-exponential term is proportional to $[DOS]_0$ via the constant $Y_{sulfate}$, and k is the apparent pseudo-first-order rate constant. We defined $Y_{sulfate}$ as the fractional yield of sulfate, thus the moles of sulfate produced per mole of DOS that reacts.

$$\Delta[SO_4^{2-}]_t = [SO_4^{2-}]_t - [SO_4^{2-}]_0 = [DOS]_0 Y_{sulfate}(1 - e^{-kt}) \quad (1)$$

Apparent first-order kinetic behavior is a common feature of complex chemical mixtures,[17] and has already been reported for DOC.[18] For each field-collected and reference DOM sample, the initial sulfate production rate ($R^0_{sulfate}$, in µmol L^{-1} h^{-1}), which is defined as the product of the initial rate of light absorption (R^0_{abs}) and the quantum yield of sulfate production ($\Phi_{sulfate}$), was calculated according to equation (2) using the parameters obtained from the non-linear fit.

$$R^0_{sulfate} = R^0_{abs}\Phi_{sulfate} = kY_{sulfate}[DOS]_0 \quad (2)$$

$R^0_{sulfate}$ varied among the nineteen samples both as a function of $[DOS]_0$ and as a function of the apparent rate constant (Table S1). Despite of these variations, a significant correlation was found between $R^0_{sulfate}$ and $[DOS]_0$ when excluding the porewater samples (N = 17, R^2 = 0.95; Figure 2B), revealing that the photochemical reactivity of DOS is overall comparable across a wide range of environments. The porewater samples displayed higher apparent rate constants, further confirming the high photochemical reactivity of DOS in these samples in correlation with the increased proportion of reduced S species (*vide supra*).

The same trend reported in Figure 1B was observed when the initial sulfate production quantum yield ($\Phi^0_{sulfate}$, *i.e.*, moles of sulfate produced per moles of photons absorbed) was plotted against

$[DOS]_0$ (Figure S2A). The fact that $\Phi^0_{sulfate}$ (thus $R^0_{sulfate}$; see equation (2)) depends on $[DOS]_0$ can be justified considering some basic principles of photochemical kinetics. We reasoned that whether sulfate is produced via direct or indirect photolysis, its quantum yield is expected to increase linearly with $[DOS]_0$. For instance, for a generic indirect process mediated by a photochemically produced reactive intermediate (PPRI), $\Phi_{sulfate}$ can be described by the following equation.

$$\Phi_{\mathrm{sulfate}} = \Phi_{\mathrm{PPRI}} \cdot \frac{k^{\mathrm{PPRI}}_{rxn,\mathrm{DOS}}[\mathrm{DOS}]_0}{k^{\mathrm{PPRI}}_d} \cdot Y^{\mathrm{PPRI}}_{\mathrm{sulfate}} \quad (3)$$

where Φ_{PPRI} is the PPRI production quantum yield, $k^{PPRI}_{rxn,DOS}$ is the bimolecular rate constant for the reaction with DOS, k^{PPRI}_d is the total deactivation rate constant, and $Y^{PPRI}_{sulfate}$ is the fractional yield of sulfate formed via reaction with PPRI. Comparable equations can be derived for direct photolysis or for a combination of direct and indirect photolysis (Supplementary Text S1).

Photochemical production of other S-containing low molecular weight compounds from DOS

To investigate whether other non-volatile DOS products are formed during UVB irradiation, the samples were also analyzed by high-performance liquid chromatography coupled to inductively coupled plasma – tandem mass spectrometry (HPLC-ICP-MS/MS). We found methanesulfonic acid (MSA) to be a common DOS photodegradation product, given its detection in all irradiated samples at concentrations ranging from 12.6 ± 0.8 nmol L^{-1} (PO3) to 300 ± 30 nmol L^{-1} (pw P8). Similarly, methanesulfinic acid (MSIA) was observed in seventeen out of nineteen samples at concentrations up to 10 times higher than MSA (Table S2). Furthermore, some of the samples with the highest $[DOS]_0$ showed few additional peaks in their chromatograms that were not present

before irradiation (Table S2). Even though we did not identify these additional products, this result hints that sub-nanomolar concentrations of other S-containing compounds might also be produced in samples with lower $[DOS]_0$. Finally, dimethyl sulfoxide (DMSO), a known aqueous-phase DMS photooxidation product,[8,9] was never detected after irradiation, which fits the view that DMSO is a DMS-specific photooxidation product.

Total sulfur was also quantified by ICP-MS/MS before and after UVB irradiation in order to estimate the relative importance of volatile *vs* non-volatile organosulfur products. Indeed, COS and CS_2 are the only DOS photoproducts that have been reported in the literature so far.[8,19–24] Studies of COS and CS_2 photoproduction are mostly limited to coastal and open ocean environments, with a single work investigating a freshwater system (an artificial lake).[25] Based on this latter publication and on mechanistic studies showing COS production from the DOM-photosensitized degradation of cysteine, glutathione and other thiols,[26–30] which are ubiquitous compounds in the environment (Table S3 and references therein), we anticipated that these volatile compounds should also be formed during our irradiation experiments. The resulting mass balances, expressed as $[S]_{5h}/[S]_0$ ratio, were complete for most of the samples, indicating that COS and CS_2 were at most minor products (Table S1 and Figure 1B). The only notable exception was the samples collected from Étang de la Gruère, which had a $[S]_{5h}/[S]_0$ value considerably lower than unity (0.87 ± 0.01). Unfortunately, the relatively high experimental error of our method provides only an estimate of the contribution of volatile species to the inventory of DOS photoproducts. Future studies based on direct gas measurements would be needed to confirm and accurately quantify photochemical production of COS and CS_2 in (natural) freshwater environments.

In order to understand the relative importance of each degradation pathway, we estimated the product distribution in each DOM sample (Figure 2C and Table S2). Note that, due to the relatively

high experimental errors, volatile product contributions were considered only if $[S]_{5h}/[S]_0$ + error < 1. Overall, sulfate was the main photoproduct, representing 28 – 94% of the reacted DOS pool, with a median value of 75%. MSIA and MSA were 0 – 39% (median: 14%) and 1.2 – 8% (median: 3.4%) of the products, respectively, while, when considered, the volatile species represented 15 – 71% of the reacted pool (median: 34%).

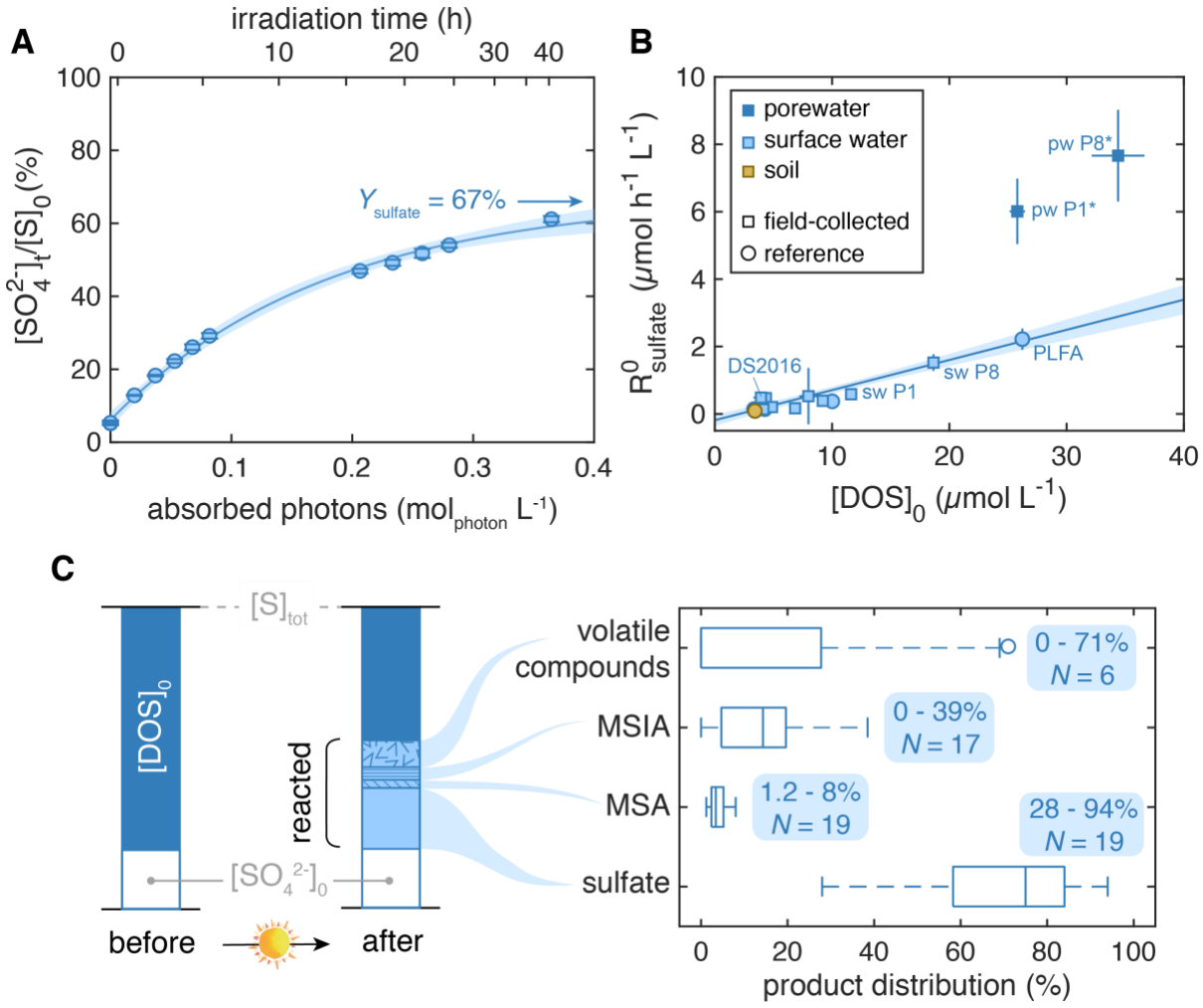

Figure 2 Long-term PLFA degradation kinetics and sulfate, MSA and MSIA production from naturally-occurring DOS. A Long-term photomineralization for PLFA. The derivation of the lower x-axis (absorbed photons) is described in the Supplementary Text S5. The error bars are standard deviations of triplicate experiments. **B** Linear regressions of $R^0_{sulfate}$ *vs* $[DOS]_0$ for the field-collected (squares) and reference (circles) surface water and soil DOM (R^2 = 0.95, N = 17). The porewater samples (blue filled squares) are excluded from the fit. When not visible, the error bars are within the symbols. Numerical values of $R^0_{sulfate}$ and $[DOS]_0$ and their associated errors are listed in Table S1. **C** Box plot showing the products distribution for the nineteen samples

investigated. The numbers in blue show the ranges for each single product, while *N* indicates the number of DOM samples in which the product was observed after irradiation. The numerical values for each DOM sample are listed in Table S2.

Environmentally relevant molecular precursor of sulfate and MSA

In order to identify possible molecular precursor substrates for sulfate and MSA production, twenty-two organic sulfur model compounds (Figure S4) were irradiated with UVB light in the presence of a natural sensitizer (Dismal Swamp water) and both sulfate and MSA were quantified via ion chromatography (Table 1 and Figure S5). The model compounds were selected based on the oxidation state of the S atom(s) and the aliphatic/aromatic nature of the carbon scaffold. Specifically, we focused on the three most abundant S oxidation states found in natural organic matter (Figure S6 and references therein), namely S(-II) (thiols, thioethers and thiophenes), S(+IV) (sulfonic acids) and S(+VI) (organosulfates). For each S oxidation state, several aromatic and aliphatic compounds were selected in order to test whether the molecular structure influences the photochemical fate of the S atom(s). Altogether, this collection of model compounds includes molecules that have already been detected in the environment or that might be present in DOS with a modified carbon scaffold (Tables S3-S4).

Table 1 Photosensitized production of sulfate and MSA from individual model compounds. Summary of sulfate and MSA concentrations detected after 2 hours of UVB irradiation (I_λ = 64 ± 4 J s^{-1} m^{-2}) in the presence of an individual model compound (50 µmol L^{-1}) and a natural sensitizer (Dismal Swamp water). The molecular structures are provided in Figure S4 and the 5-hour irradiation kinetics in Figure S5. N.D. = no peak detected; N.S. = non-significant ($[SO_4^{2-}]_{corr,2h}$ < 0.0 ± 0.2 µmol L^{-1}). [a] Hybridization of carbon atoms bound to sulfur referred to as aliphatic (sp^3) or aromatic (sp^2) in the main text. [b] Corrected for the sulfate produced by the natural sensitizer. [c] + = detected in the environment (references in Table S3); * = surrogate for S-containing functional groups present in environmental systems (see Table S4 for examples). [d] 50 mg_C L^{-1} addition of bovine serum albumin is equivalent to ≈ 25 μmol_S L^{-1}.

Compound	C hybridization [a]	$[SO_4^{2-}]_{corr,2h}$ (µmol L^{-1}) [b]	$[MSA]_{2h}$ (µmol L^{-1})	Environmental occurrence [c]

S(-II): Thiols, thioethers and thiophenes				
Cysteine	sp^3	**2.2** ± 0.2	N.D.	+
Methionine	sp^3	**1.87** ± 0.03	**1.97** ± 0.02	+
Glutathione	sp^3	**2.5** ± 0.4	N.D.	+
Bovine serum albumin [d]	sp^3	**1.1** ± 0.4	N.D.	*
3-Mercaptopropionic acid	sp^3	**1.08** ± 0.02	N.D.	+
Biotin	sp^3	**2.6** ± 0.2	N.D.	+
Thioacetamide	sp^2	**7.3** ± 0.3	N.D.	*
3-(Methylthio)benzoic acid	sp^2/sp^3	**0.25** ± 0.05	**4.5** ± 0.8	*
Thioanisole	sp^2/sp^3	**1.00** ± 0.02	**0.62** ± 0.01	+
3-Mercaptobenzoic acid	sp^2	**3.4** ± 0.3	N.D.	*
Bithiophene	sp^2	**20** ± 3	N.D.	*
S(+IV): Sulfonic acids				
Cysteine sulfonic acid	sp^3	N.S.	N.D.	*
Methanesulfonic acid	sp^3	N.S.	N.D.	+
1-Hexanesulfonic acid	sp^3	N.S.	N.D.	*
2-(Cyclohexylamino)ethane sulfonic acid	sp^3	N.S.	N.D.	*
Taurocholate	sp^3	N.S.	N.D.	*
Benzenesulfonic acid	sp^2	**1.5** ± 0.1	N.D.	*
p-Toluenesulfonic acid	sp^2	**4.3** ± 0.2	N.D.	+
Naphthoquinonesulfonic acid	sp^2	**35** ± 2	N.D.	*
4-Dodecylbenzenesulfonic acid	sp^2	**1.2** ± 0.1	N.D.	+
S(+VI): Organosulfates				
Pegnenolone sulfate	-	**3.0** ± 0.1	N.D.	*
4-Nitrocathechol sulfate	-	**3.7** ± 0.1	N.D.	*

Nearly all model compounds could be photomineralized to sulfate, albeit with different kinetics and different yields (Figure S5). The aliphatic sulfonic acids were the only molecules that showed no sulfate production. In two cases (cysteine sulfonic acid and MSA), we could confirm experimentally the photochemical stability of the parent compound ($[MSA]_{5h}/[MSA]_{0h}$ = 1.00 ±

0.06; $[CysSO_3H]_{5h}/[CysSO_3H]_{0h} = 1.03 \pm 0.04$), providing good support for the hypothesis that the incomplete conversion of DOS to sulfate can also be due to the initial presence and/or formation of photochemically stable DOS components. Such photorecalcitrant molecules can be produced from biological activity (*i.e.*, cysteine sulfonic acid)[31] or could be formed during DOS photodegradation (*i.e.*, MSA). In addition, MSA was always formed during the photodegradation of methyl thioethers, suggesting that methionine and other naturally occurring methyl thioethers can be the precursors of MSA. In one case, MSA was produced in higher yields than sulfate (3-(methylthio)benzoic acid: $[SO_4^{2-}]_{corr,2h} = 0.25 \pm 0.05$ µmol L^{-1}; $[MSA]_{2h} = 4.5 \pm 0.8$ µmol L^{-1}), reinforcing the idea that photomineralization of DOS to sulfate is not necessarily quantitative.

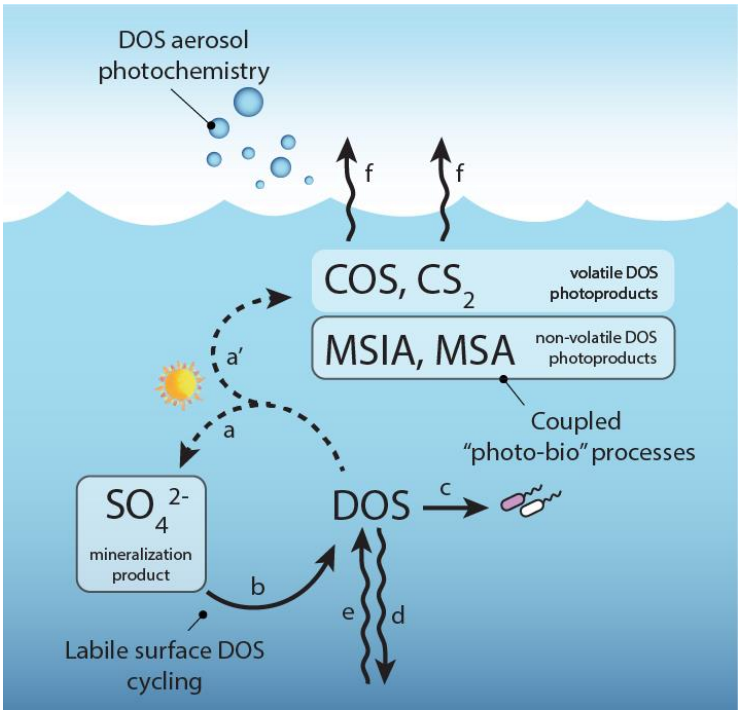

Figure 3. Overview of the DOS cycle in sunlit surface waters and possible implications for DOS biogeochemistry. The dotted lines represent photochemical processes. The photoproducts identified for the first time in this study are in black-framed boxes. *Legend*: *a.* photomineralization; *a'.* photofragmentation; *b.* sulfate assimilation and DOS release from phytoplankton; *c.* microbial DOS uptake; *d.* downwelling; *e.* upwelling; *f.* outgassing.

Implications for the sulfur cycle

Our study reports the first direct evidence of sulfate production from the photochemical degradation of dissolved organic sulfur from a variety of natural water samples (Figure 3). This finding fills in the general picture of the role of photochemistry on the biogeochemical cycle of the main elements, showing that, similar to dissolved organic carbon[8], nitrogen[32,33] and phosphorous[34], also DOS can be converted to its inorganic form via photochemical routes. Such processes are vital in releasing valuable elements tied up in recalcitrant forms, and thus can stimulate the flow and the recycling of elements across environmental compartments.

In addition, the identification of a photomineralization mechanism provides a more complete picture on the biogeochemistry of DOS. Only few studies on DOS photodegradation can be found in the literature,[5–7] which all focus on the loss of DOS formulas via HRMS, and not on the identification of the S-containing products. The inverse is true for the studies of photochemical formation of COS and CS_2 in the natural environment,[8,19–24] which describe the appearance of products with no clear link made to loss of DOS. Our work provides a bridge between these two research themes. First, it suggests that sulfate is the most likely product associated to the loss of DOS observed in the HRMS studies. For instance, Gomez-Saez et al. reported up to ≈ 30% of $[DOS]_0$ loss after 2 days of solar irradiation in saltmarsh porewater samples. Even though care should be taken when comparing results obtained with different light sources, this number qualitatively agrees with the high mineralized fractions (*i.e.*, DOS conversion to sulfate) that we observed for our porewater samples (*i.e.*, $f_{photo,5h}$ = 50 – 52%). Second, the present work gives a sense of the relative importance of the different degradation pathways. In particular, we found that sulfate is the main photodegradation product, while the other volatile (COS, CS_2) and non-volatile

(MSA, MSIA) low-molecular weight compounds are quantitatively less important. Our results are directly relevant to aquatic terrestrial organic matter in freshwater systems, but we expect them to hold valid also for marine DOM. Control experiments showed no suppression in sulfate production at high ionic strength and low DOC concentrations, which are conditions typical of marine environments (Supplementary Text S2). In addition, preliminary results with a marine DOM sample collected in the Pacific Ocean were found in good agreement with the findings presented in this work for terrestrial DOM and PLFA (Supplementary Text S2). As a further point, model compounds able to produce both sulfate and COS are present in both terrestrial and marine environments (Table S3). For instance, glutathione, which can produce both COS[27,30] and sulfate (*vide supra*), is commonly found in freshwater,[35] estuaries[36] and in the open ocean[37]. Nevertheless, further studies need to confirm experimentally the production of sulfate and non-volatile low-molecular weight compounds from marine DOS photolysis.

The discovery of several photodegradation routes puts the DOS cycle into a new perspective, providing possible answers to the many unresolved questions on its biogeochemistry and suggesting new research directions (Figure 3). For example, photomineralization can be a potential explanation for the fast DOS turnover observed by Ksionzek *et al.* in the mixed surface layer of the ocean.[4] In particular, we anticipate that autochthonous DOS released by phytoplankton at the surface (*i.e.*, glutathione and other peptides) can be converted to sulfate upon DOM-sensitized photolysis. In addition, photochemistry can play a role in converting recalcitrant DOS components into bioavailable substrates, similarly to what happens for carbon cycling.[8,38] Indeed, microorganisms able to use MSA either as a S-source, a C-source or an energy source have been identified in a variety of environments[39,40] and were recently found to be abundant in surface seawater[41]. Lastly, we hypothesize that non-DMS organosulfur compounds present in aerosols,

such as organosulfates[42], and cysteine- and methionine-containing peptides and proteins [38], might degrade to sulfate via aqueous phase photochemical reactions sensitized by organic chromophores, similar to what we report here for bulk solutions. Thus, atmospheric DOS might be an aqueous-phase precursor of non-sea-salt sulfate (nss-SO_4^{2-}), an important contributor to aerosol formation in remote marine areas.[3,44] Future work is needed to assess the importance of DOS photodegradation in the ocean surface and in the atmosphere.

Methods

Materials

The twenty-two DOS model compounds were purchased from commercial vendors. Specifically, *L*-cysteine (≥ 99.5%), *L*-cysteine sulfonic acid monohydrate (≥ 99%), sodium 1-hexanesulfonate monohydrate (≥ 99%), 2-(cyclohexylamino)ethanesulfonic acid (≥ 99.5%) and sodium taurocholate were purchased from Fluka. *L*-Gluthatione (≥ 98%), *L*-methionine (≥ 98%), bovine serum albumin (≥ 98%), 3-mercaptopropionic acid (≥ 99%), thioacetamide (≥ 99%), 3-mercaptobenzoic acid (95%), 3-(methylthio)benzoic acid (97%), *D*-biotin (≥ 99%), 2,2'-bithiophene (≥ 98.5%), methanesulfonic acid (99%), 1,2-naphthoquinone-4-sulfonic acid sodium salt (97%), sodium benzene sulfonate (97%), sodium dodecyl benzene sulfonate (technical grade), 4-nitrocathechol sulfate dipotassium salt (99%), pregnenolone sulfate sodium salt (≥ 98%), thioanisole (≥ 99%) were obtained from Sigma Aldrich, while 4-toluensulfonic acid monohydrate (≥ 98%) was obtained from TCI. For each compound, a stock solution (10 mmol L^{-1}) was prepared in nanopure water (resistivity > 18 MΩ, Barnstead nanopure System). When required, acetonitrile was added as a cosolvent (LiChrosolv, HPLC grade, 20% to 100%). The stock solutions were

305 stored at 4 °C until use. The irradiation experiments were performed on solutions containing 50
306 µmol L^{-1} (50 mg_C L^{-1} for bovine serum albumin) of a given DOS-model compound in Dismal
307 Swamp water (DS2014, 20 mg_C L^{-1}).

308 The actinometry compounds, 4-nitroanisole (PNA, 97%) and pyridine (≥ 99.9%), were also
309 obtained from Sigma Aldrich. PNA was recrystallized from ether prior to use. Dimethyl sulfoxide
310 (DMSO, ≥ 99%) and sodium methane sulfinate (85%, technical grade) were also purchased from
311 Sigma Aldrich. Potassium sulfate (≥ 99%) was obtained from Merck, while sodium chloride (ACS
312 reagent) was from Fluka.

313 Eight reference DOM samples were obtained from the International Humic Standard Society
314 (IHSS, St. Paul, Minnesota): Elliott Soil Humic Acid (ESHA, 1S102H), Mississippi River Natural
315 Organic Matter (MRNOM, 1R110N), Nordic Aquatic Humic Acid (NAHA, 1R105H), Nordic
316 Aquatic Fulvic Acid (NAFA, 1R105F), Pony Lake Fulvic Acid (PLFA, 1R109F), Suwannee River
317 Fulvic Acid (SRFA, 2S101F), Suwannee River Humic Acid (SRHA, 2S101H) and Suwannee
318 River Natural Organic Matter (SRNOM, 1R101N). Dissolved organic matter (DOM) stock
319 solutions of approximately 300 mg L^{-1} (≈ 150 mg_C L^{-1}) were prepared in nanopure water by
320 stepwise addition of NaOH 1 mol L^{-1} until reaching a pH value of 10. The stock solutions were
321 then adjusted to pH 7 upon addition of HCl 1 mol L^{-1}, and frozen at -20 °C until use. Solutions
322 containing 20 mg_C L^{-1} were prepared by dilution of the concentrated stocks with nanopure water
323 shortly before the irradiation experiments.

324 The ten natural waters were collected from the following sites: Great Dismal Swamp, Suffolk,
325 Virginia, USA (two surface water samples, collected in summer in 2014 and 2016; DS2014 and
326 DS2016); Étang de la Gruyère, Switzerland (one surface water sample, collected in May 2015;
327 EG); Lake Bradford, Tallahassee, Florida, USA (one surface water sample, collected in December

2015; LB); Storhultsmossen peat bog, Sweden (two surface water samples from two pools of the bog, collected in July 2016; PO1 and PO3); Prairie Pothole peat bogs, U.S. Geological Survey Cottonwood Lakes study area, Jamestown, North Dakota, USA (two surface water samples and two porewater samples from two different pools, collected in November 2014; sw P1, sw P8, pw P1, pw P8). The two Great Dismal Swamp, the Étang de la Gruère and the Lake Bradford water samples were filtered shortly after collection (Whatman Polycap TC 75, pore size 0.2 µm) and stored at 4˚C until use. The four Prairie Pothole water samples were subjected to solid phase extraction (SPE) to remove the natural background of sulfate. The details of the extraction procedure are provided in the Supplementary Text S3. Additional information on the collection and handling of the original water samples can be found in Walpen *et al.*[45] (Storhultsmossen bog), Wallace *et al.*[46] (Prairie Pothole Peat porewaters) or McCabe and Arnold[47] (Prairie Pothole Peat surface waters). For the irradiation experiments, the two Dismal Swamp waters and the four Prairie Pothole Peat extracts were diluted to approximately 20 $mg_C\ L^{-1}$ in nanopure water. A Dismal Swamp solution (DS2014, 20 $mg_C\ L^{-1}$) was also amended with 10 $mg_C\ L^{-1}$ of bovine serum albumin (BSA), which was used here as a surrogate of microbially derived DOM (*i.e.*, proteins). The Étang de la Gruère, the two Storhultsmossen and Lake Bradford waters were used undiluted.

Photodegradation experiments

The photolysis experiments were performed on reference DOM samples and on field-collected natural waters or their SPE extracts at a concentration of ≈ 20 $mg_C\ L^{-1}$ (*natural water experiments*), or on solutions containing Dismal Swamp as natural sensitizer (DS2014, ≈ 20 $mg_C\ L^{-1}$) and the selected DOS model compound (50 µmol L^{-1}) (*model compounds experiments*). The natural water experiments were performed at least in triplicates, while the model compounds experiments at

least in duplicate. A summary of the initial dissolved organic carbon (DOC) and sulfate concentrations for the nineteen experimental solutions is provided in Table S5.

The solutions (10 mL) were placed in cork-stoppered borosilicate test tubes (Pyrex, 15 × 85 mm, disposable) and were irradiated for 5 hours inside a photoreactor (Rayonet, Southern New England Ultraviolet Co) equipped with 6 × 300 nm light bulbs (Southern New England Ultraviolet Co, RPR-3000 A lamps) and a turntable. During irradiation, a fan was turned on to keep the temperature constant around 30-32 °C. At each hour, an aliquot was withdrawn for quantification of sulfate via ion chromatography (IC). In the model compound experiments, MSA was also quantified via IC. For the quantification of volatile and non-volatile DOS products in the natural water experiments, an aliquot was withdrawn at the beginning and at the end of the irradiation. Total S was quantified via ICP-MS/MS, while MSA and MSIA were quantified by HPLC-ICP-MS/MS.

The light intensity inside the photoreactor was monitored with the chemical actinometer pyridine/*p*-nitroanisole (py/PNA).[48] A solution containing 20 μmol L^{-1} of PNA and 0.25 mmol L^{-1} of pyridine in nanopure water was irradiated for 5 hours in the experimental conditions described above. PNA and pyridine were quantified via ultra-performance liquid chromatography (UPLC) with UV detection. For the sulfate production experiments from DOM and model compounds, we calculated an integrated irradiance of 64 ± 4 J s^{-1} m^{-2} ($\Delta\lambda$ = 290 – 400 nm, Figure S7), while for experiments investigating volatile compounds, MSA and MSIA production from natural DOM, the irradiance over the same wavelength range was 45 ± 4 J s^{-1} m^{-2}. More details can be found in the Supplementary Text S4.

Control experiments. Control experiments were also performed to unambiguously attribute sulfate, MSA or MSIA production to photochemical processes. As a dark control, we placed aluminum

foil-covered test tubes in the photoreactor for 5 hours. No thermal degradation could be observed for any of the natural waters or the model compounds. Oxygen concentrations were also monitored to confirm that anoxic conditions, which are not expected on the surface of water bodies, were never present during our irradiation experiments. Since acetonitrile was used as a co-solvent in the preparation of some DOS model compound stock solutions, DS2014 was amended with up to 0.5% v/v acetonitrile and we confirmed that photochemical production of sulfate was unaffected. We also tested the effect of small methanol concentrations on sulfate production rates, as methanol was used as solid phase extraction solvent and trace amounts might be present in the final extracts. A small rate decrease was observed for DS2014 in the presence of methanol, even though for concentrations below 0.5% v/v the rate variation was within the statistical error. This result suggests that, in the worst case, trace amounts of methanol might cause an underestimation of sulfate production rates. In order to account for potential artifacts introduced by the solid phase extraction procedure, Dismal Swamp water was subjected to the same SPE protocol of the Prairie Pothole samples. As the only effect, the extraction resulted in an increase of DOC/DOS ratio (*i.e.*, caused an enrichment in DOC), which slightly reduced the sulfate production rate in the extracted DS sample compared to the unextracted one. We also conducted additional experiments to show that sulfate production from DOS is in principle possible under with natural sunlight (*i.e.*, at $\lambda >$ 300 nm) and in the marine environment. The detailed description of the control experiments is provided in the Supplementary Text S2.

Chemical analyses

Sulfate and MSA quantification via ion chromatography (IC). Sulfate and MSA were quantified via ion chromatography using either a DX-320 IC instrument (Thermo Scientific, Sunnyvale, CA, USA), or a 940 Professional IC Vario instrument (Metrohm). The DX-320 system was equipped

with an EG40 eluent gradient generator, a Dionex Ion Pack AG11-HC RFIC 4 mm column and guard column, a Dionex AERS 500 4 mm electric suppressor and an electrical conductivity detector. The sample injection volume was 250 µL, the flow rate was 1.5 mL min^{-1} and the following KOH gradient was used: 0 – 11 min, 1 mmol L^{-1}; 11 – 37 min, 1 mmol L^{-1} to 40 mmol L^{-1}; 37 to 38 min, 40 mmol L^{-1}; 38 to 41 min, 1 mmol L^{-1}. In these conditions, sulfate was eluted at 24.0 min. The Metrohm system was equipped with a Metrosep A Supp 5-250/4.0 column thermostated at 30˚C, a conductivity detector, a chemical suppressor and was run in isocratic mode. The mobile phase was $NaHCO_3$ 0.8 mmol L^{-1} + Na_2CO_3 2.9 mmol L^{-1} prepared in nanopure water and delivered at a flow rate of 0.7 mL min^{-1}, while the sample injection volume was 100 µL. In these conditions sulfate was eluted at 25.5 min. The two IC systems provided reproducible and comparable results and were used interchangeably for sulfate detection. The DX-320 instrument was also employed for the detection of MSA in the model compounds experiments (12.5 min retention time in the conditions described above), but it was unsuitable for MSA quantification in the natural water experiments due to the relatively high detection limits (≈ 0.2 µmol L^{-1}). In addition, MSA analysis was not possible with the Metrohm IC systems as MSA co-eluted with acetate, a common DOM photolysis product.[49]

Total sulfur determination via ICP-MS/MS. Total sulfur concentrations were measured using an Agilent 8900 inductively coupled plasma – tandem mass spectrometry (ICP-MS/MS) instrument equipped with a collision/reaction cell (C/RC) (Agilent Technologies, Switzerland). We used the integrated sample introduction system (ISIS), a Micromist nebulizer, a Scott double pass spray chamber, and platinum sampler and skimmer cones. Sulfur was detected in MS/MS mode using oxygen in the C/RC. The acquisition parameters were as follows: *m/z* 32 (MS^1) - 48 (MS^2), as S formed $^{32}S^{16}O^+$ in the C/RC in presence of oxygen, integration time 0.05 ms, 1 point per peak,

three replicates and 100 sweeps/replicate. All ICP-MS/MS parameters were optimized daily using a solution containing 1 µg L^{-1} of Li, Co, Y, Tl, and Ce. Only the gas flow rate and the energy discrimination were set to 30% O_2 with 2 mL min^{-1} H_2 and -8 V. An internal standard containing Sc (1 mg L^{-1}), In (1 mg L^{-1}) and Lu (1 mg L^{-1}) was used to check the stability of the signal during the runs. Quantification was done by external calibrations using standards prepared in nanopure water. The detection limit was 6 nmol L^{-1}. The natural water samples were diluted to be in the concentration range of 1.2 – 0.012 µmol L^{-1}.

MSA, MSIA, DMSO quantification via HPLC-ICP-MS/MS. Sulfur speciation analysis via HPLC-ICP-MS/MS was performed using an Agilent 1200 series HPLC pump and the Agilent 8900 ICP-MS/MS instrument described above. The chromatographic separation was performed with an Hypercarb 4.6x100 mm, particle size 5 µm column (Thermo Fisher) and an elution gradient based on changes in formic acid concentration (24 - 240 mmol L^{-1}). The mobile phase was delivered at 1 mL min^{-1} and the sample injection volume was 100 µL. As for total S quantification, S speciation was analyzed in MS/MS mode using oxygen in the C/RC, following the same tuning procedure and C/RC settings. The acquisition parameters were *m/z* 32 – 48 and an integration time of 0.05 ms. An internal standard containing Sc (5 mg L^{-1}) and Y (5 mg L^{-1}) was delivered post-column using a T-connector and the peristaltic pump of the ICP-MS/MS. This allowed to monitor the signal stability during the analyses. Quantification of MSA and MSIA was done by external calibrations using standards prepared in nanopure water. Detection limits were 7 nmol L^{-1} for MSA and 38 nmol L^{-1} for MSIA. The experimental samples were analyzed undiluted.

Other analyses. Total non-purgeable organic carbon (TOC) was determined using a TOC analyzer (Shimadzu Corporation). PNA and pyridine concentrations were measured with a Waters ACQUITY UPLC system equipped with a C18 column (ACQUITY UPLC BEH 130 C18, 1.7 µm;

2.1 × 150 mm) and its guard column (ACQUITY UPLC BEH C18 VanGuard Pre-column, 130Å, 1.7 µm, 2.1 mm × 5 mm). The analyses were performed in isocratic mode using a mixture of 40% acetate buffer pH 6 (+ 10% acetonitrile) and 60% acetonitrile as eluent, a flow rate of 0.15 mL min^{-1}, 5 µL injection volume and UV-Vis detection at 310 and 250 nm for PNA and pyridine, respectively. UV-Vis spectra were recorded with a Cary 100 Bio Spectrophotometer (Varian) using a 1 cm pathlength quartz cuvette in double beam mode.

Data analysis

Natural waters experiments. For each individual experiment, the concentration of photoproduced sulfate at time *t* ($\Delta[SO_4^{2-}]_t$) was calculated according to equation (4), where $[SO_4^{2-}]_0$ is the initial sulfate concentration.

$$\Delta[SO_4^{2-}]_t = [SO_4^{2-}]_t - [SO_4^{2-}]_0 \quad (4)$$

For each field-collected water or reference DOM sample, $\Delta[SO_4^{2-}]_t$ values from independent triplicate experiments were averaged and the associated standard deviation was calculated. The averaged $\Delta[SO_4^{2-}]_t$ values over 5 hours of UVB irradiation were fitted with a monoexponential growth function (equation (1)) using a weighted non-linear fit (Matlab R2018b). From the fitting, the initial sulfate production rate ($R^0_{sulfate}$, in mmol L^{-1} h^{-1}) was calculated from the product of the fitting parameters (equation (2)). A summary of $R^0_{sulfate}$ values or the nineteen field-collected and reference DOM samples is provided in Table S1. The initial sulfate production quantum yield ($\Phi^0_{sulfate}$) was obtained from the same dataset using as x-axis the absorbed photons instead of the time (Supplementary Text S5). The results are provided in Table S1 and Figure S2.

For the 5-hour time point, the fraction of the initial DOS converted to sulfate ($f_{sulfate,5h}$) was calculated according to equation (5) (Table S1).

$$f_{\text{sulfate,5h}} = \frac{\Delta[\text{SO}_4^{2-}]_{\text{5h}}}{[\text{DOS}]_0} \quad (5)$$

where $\Delta[SO_4^{2-}]_{5h}$ is the photoproduced sulfate according to equation (4) and $[DOS]_0$ is the initial DOS concentration. $[DOS]_0$ was calculated according to equation (6),[4,19] where $[S]_0$ was obtained via ICP-MS/MS and $[SO_4^{2-}]_0$ via ion chromatography. The values of $[DOS]_0$ for the individual samples are listed in Table S1.

$$[\text{DOS}]_0 = [\text{S}]_0 - [\text{SO}_4^{2-}]_0 \quad (6)$$

The product distribution was calculated according to equation (7), where $[volatiles]_{5h} = 1 - [S]_{5h}/[S]_0$. Note that $[volatiles]_{5h}$ was set to zero if $[S]_{5h}/[S]_0$ + error ≥ 1, thus it was considered only for the six waters indicated with one or two asterisks in Figure 1B.

$$\%\text{X} = \frac{[\text{X}]_{\text{5h}}}{\Delta[\text{SO}_4^{2-}]_{\text{5h}} + [\text{MSA}]_{\text{5h}} + [\text{MSIA}]_{\text{5h}} + [\text{volatiles}]_{\text{5h}}} \quad (7)$$

Model compounds experiments. In the model compounds experiments, sulfate photoproduction was corrected for the background of the natural sensitizer (DS2014) according to equation (8).

$$[\text{SO}_4^{2-}]_{corr} = \Delta[\text{SO}_4^{2-}]_t - \Delta[\text{SO}_4^{2-}]_{t,\text{DS2014}} \quad (8)$$

where $\Delta[SO_4^{2-}]_{t,DS2014}$ is the photoproduced sulfate at time *t* generated from the natural sensitizer in the absence of amendments. For each model compound, sulfate ($[SO_4^{2-}]_{corr,2h}$) and MSA ($[MSA]_{2h}$) concentrations after 2 hours of UVB irradiation are reported in Table 1. The MSA data were not corrected due to the negligible background from the natural sensitizer in the concentration range of interest.

References and Notes

1. Lovelock, J. E., Maggs, R. J. & Rasmussen, R. A. Atmospheric Dimethyl Sulphide and the Natural Sulphur Cycle. *Nature* **237**, 453–454 (1972).
2. Charlson, R. J., Lovelock, J. E., Andreae, M. O. & Warren, S. G. Oceanic phytoplankton, atmospheric sulphur, cloud albedo and climate. *Nature* **326**, 655–661 (1987).
3. Quinn, P. K. & Bates, T. S. The case against climate regulation via oceanic phytoplankton sulphur emissions. *Nature* **480**, 51–56 (2011).
4. Ksionzek, K. B. *et al.* Dissolved organic sulfur in the ocean: Biogeochemistry of a petagram inventory. *Science* **354**, 456–459 (2016).
5. Gomez-Saez, G. V., Pohlabeln, A. M., Stubbins, A., Marsay, C. M. & Dittmar, T. Photochemical alteration of dissolved organic sulfur from sulfidic porewater. *Environ. Sci. Technol.* **51**, 14144–14154 (2017).
6. Stubbins, A. & Dittmar, T. Illuminating the deep: Molecular signatures of photochemical alteration of dissolved organic matter from North Atlantic Deep Water. *Mar. Chem.* **177**, 318–324 (2015).
7. Herzsprung, P., Hertkorn, N., Friese, K. & Schmitt-Kopplin, P. Photochemical degradation of natural organic sulfur compounds (CHOS) from iron-rich mine pit lake pore waters--an initial understanding from evaluation of single-elemental formulae using ultra-high-resolution mass spectrometry. *Rapid Commun. Mass Spectrom. RCM* **24**, 2909–2924 (2010).
8. Mopper, K., Kieber, D. J. & Stubbins, A. Chapter 8 - Marine Photochemistry of Organic Matter: Processes and Impacts A2 - Hansell, Dennis A. in *Biogeochemistry of Marine Dissolved Organic Matter (Second Edition)* (ed. Carlson, C. A.) 389–450 (Academic Press, 2015).

9. Hoffmann, E. H. *et al.* An advanced modeling study on the impacts and atmospheric implications of multiphase dimethyl sulfide chemistry. *Proc. Natl. Acad. Sci.* **113**, 11776–11781 (2016).
10. Fimmen, R. L., Cory, R. M., Chin, Y.-P., Trouts, T. D. & McKnight, D. M. Probing the oxidation-reduction properties of terrestrially and microbially derived dissolved organic matter. *Geochim. Cosmochim. Acta* **71**, 3003–3015 (2007).
11. Liu, Z.-Q., Shah, A. D., Salhi, E., Bolotin, J. & von Gunten, U. Formation of brominated trihalomethanes during chlorination or ozonation of natural organic matter extracts and model compounds in saline water. *Water Res.* **143**, 492–502 (2018).
12. Sleighter, R. L. *et al.* Evidence of Incorporation of Abiotic S and N into Prairie Wetland Dissolved Organic Matter. *Environ. Sci. Technol. Lett.* **1**, 345–350 (2014).
13. Poulin, B. A. *et al.* Spatial Dependence of Reduced Sulfur in Everglades Dissolved Organic Matter Controlled by Sulfate Enrichment. *Environ. Sci. Technol.* **51**, 3630–3639 (2017).
14. Minor, E. C., Pothen, J., Dalzell, B. J., Abdulla, H. & Mopper, K. Effects of salinity changes on the photodegradation and ultraviolet—visible absorbance of terrestrial dissolved organic matter. *Limnol. Oceanogr.* **51**, 2181–2186 (2006).
15. Erickson, P. R. *et al.* Singlet Oxygen Phosphorescence as a Probe for Triplet-State Dissolved Organic Matter Reactivity. *Environ. Sci. Technol.* **52**, 9170–9178 (2018).
16. Sharpless, C. M. *et al.* Photooxidation-Induced Changes in Optical, Electrochemical, and Photochemical Properties of Humic Substances. *Environ. Sci. Technol.* **48**, 2688–2696 (2014).
17. Bandstra, J. Z. & Tratnyek, P. G. Central limit theorem for chemical kinetics in complex systems. *J. Math. Chem.* **37**, 409–422 (2005).

18. Mostovaya, A., Hawkes, J. A., Koehler, B., Dittmar, T. & Tranvik, L. J. Emergence of the Reactivity Continuum of Organic Matter from Kinetics of a Multitude of Individual Molecular Constituents. *Environ. Sci. Technol.* **51**, 11571–11579 (2017).
19. Cutter, G. A., Cutter, L. S. & Filippino, K. C. Sources and cycling of carbonyl sulfide in the Sargasso Sea. *Limnol. Oceanogr.* **49**, 555–565 (2004).
20. Ulshöfer, V. S., Flock, O. R., Uher, G. & Andreae, M. O. Photochemical production and air-sea exchange of carbonyl sulfide in the eastern Mediterranean Sea. *Mar. Chem.* **53**, 25–39 (1996).
21. Weiss, P. S., Andrews, S. S., Johnson, J. E. & Zafiriou, O. C. Photoproduction of carbonyl sulfide in South Pacific Ocean waters as a function of irradiation wavelength. *Geophys. Res. Lett.* **22**, 215–218 (1995).
22. Flöck, O. R. & Andreae, M. O. Photochemical and non-photochemical formation and destruction of carbonyl sulfide and methyl mercaptan in ocean waters. *Mar. Chem.* **54**, 11–26 (1996).
23. Xie, H. & Moore, R. M. Carbon disulfide in the North Atlantic and Pacific oceans. *J. Geophys. Res. Oceans* **104**, 5393–5402 (1999).
24. Uher, G. & Andreae, M. Photochemical production of carbonyl sulfide in North Sea water: A process study. *Limnol. Oceanogr.* **42**, 432–442 (2003).
25. Du, Q. *et al.* Photochemical production of carbonyl sulfide, carbon disulfide and dimethyl sulfide in a lake water. *J. Environ. Sci.* **51**, 146–156 (2017).
26. Pos, W. H., Riemer, D. D. & Zika, R. G. Carbonyl sulfide (OCS) and carbon monoxide (CO) in natural waters: evidence of a coupled production pathway. *Mar. Chem.* **62**, 89–101 (1998).

27. Andreae, M. O. & Ferek, R. J. Photochemical production of carbonyl sulphide in marine surface waters. *Nature* **307**, 148 (1984).
28. Zepp, R. G. & Andreae, M. O. Factors affecting the photochemical production of carbonyl sulfide in seawater. *Geophys. Res. Lett.* **21**, 2813–2816 (1994).
29. Modiri Gharehveran, M. & Shah, A. D. Indirect Photochemical Formation of Carbonyl Sulfide and Carbon Disulfide in Natural Waters: Role of Organic Sulfur Precursors, Water Quality Constituents, and Temperature. *Environ. Sci. Technol.* **52**, 9108–9117 (2018).
30. Flöck, O. R., Andreae, M. O. & Dräger, M. Environmentally relevant precursors of carbonyl sulfide in aquatic systems. *Mar. Chem.* **59**, 71–85 (1997).
31. Kelly, D. P. & Smith, N. A. Organic Sulfur Compounds in the Environment Biogeochemistry, Microbiology, and Ecological Aspects. in *Advances in Microbial Ecology* 345–385 (Springer, Boston, MA, 1990). doi:10.1007/978-1-4684-7612-5_9
32. Vähätalo, A. V. & Zepp, R. G. Photochemical Mineralization of Dissolved Organic Nitrogen to Ammonium in the Baltic Sea. *Environ. Sci. Technol.* **39**, 6985–6992 (2005).
33. Bushaw, K. L. *et al.* Photochemical release of biologically available nitrogen from aquatic dissolved organic matter. *Nature* **381**, 404–407 (1996).
34. Gardolinski, P. C. F. C., Worsfold, P. J. & McKelvie, I. D. Seawater induced release and transformation of organic and inorganic phosphorus from river sediments. *Water Res.* **38**, 688–692 (2004).
35. Hu, H., Mylon, S. E. & Benoit, G. Distribution of the thiols glutathione and 3-mercaptopropionic acid in Connecticut lakes. *Limnol. Oceanogr.* **51**, 2763–2774 (2006).

36. Dupont, C. L., Moffett, James. W., Bidigare, R. R. & Ahner, B. A. Distributions of dissolved and particulate biogenic thiols in the subartic Pacific Ocean. *Deep Sea Res. Part Oceanogr. Res. Pap.* **53**, 1961–1974 (2006).
37. Tang, D., Hung, C.-C., Warnken, K. W. & Santschi, P. H. The distribution of biogenic thiols in surface waters of Galveston Bay. *Limnol. Oceanogr.* **45**, 1289–1297 (2000).
38. Cory, R. M. & Kling, G. W. Interactions between sunlight and microorganisms influence dissolved organic matter degradation along the aquatic continuum. *Limnol. Oceanogr. Lett.* **3**, 102–116 (2018).
39. Baker, S. C., Kelly, D. P. & Murrell, J. C. Microbial degradation of methanesulphonic acid: a missing link in the biogeochemical sulphur cycle. *Nature* **350**, 627–628 (1991).
40. Kelly, D. P. & Murrell, J. C. Microbial metabolism of methanesulfonic acid. *Arch. Microbiol.* **172**, 341–348 (1999).
41. Henriques, A. C. & Marco, P. D. Methanesulfonate (MSA) Catabolic Genes from Marine and Estuarine Bacteria. *PLOS ONE* **10**, e0125735 (2015).
42. McNeill, V. F. Aqueous Organic Chemistry in the Atmosphere: Sources and Chemical Processing of Organic Aerosols. *Environ. Sci. Technol.* **49**, 1237–1244 (2015).
43. Quinn, P. K., Collins, D. B., Grassian, V. H., Prather, K. A. & Bates, T. S. Chemistry and Related Properties of Freshly Emitted Sea Spray Aerosol. *Chem. Rev.* **115**, 4383–4399 (2015).
44. Quinn, P. K., Coffman, D. J., Johnson, J. E., Upchurch, L. M. & Bates, T. S. Small fraction of marine cloud condensation nuclei made up of sea spray aerosol. *Nat. Geosci.* **10**, 674–679 (2017).

45. Walpen, N., Getzinger, G. J., Schroth, M. H. & Sander, M. Electron-donating Phenolic and Electron-accepting Quinone Moieties in Peat Dissolved Organic Matter: Quantities and Redox Transformations in the Context of Peat Biogeochemistry. *Environ. Sci. Technol.* **52**, 5236–5245 (2018).
46. Wallace, G. C., Sander, M., Chin, Y.-P. & Arnold, W. A. Quantifying the electron donating capacities of sulfide and dissolved organic matter in sediment pore waters of wetlands. *Environ. Sci. Process. Impacts* **19**, 758–767 (2017).
47. McCabe, A. J. & Arnold, W. A. Seasonal and spatial variabilities in the water chemistry of prairie pothole wetlands influence the photoproduction of reactive intermediates. *Chemosphere* **155**, 640–647 (2016).
48. Laszakovits, J. R. *et al.* p-Nitroanisole/Pyridine and p-Nitroacetophenone/Pyridine Actinometers Revisited: Quantum Yield in Comparison to Ferrioxalate. *Environ. Sci. Technol. Lett.* **4**, 11–14 (2016).
49. Moran, M. A. & Zepp, R. G. Role of photoreactions in the formation of biologically labile compounds from dissolved organic matter. *Limnol. Oceanogr.* **42**, 1307–1316 (1997).

Acknowledgements: The authors thank Dr. N. Borduas-Dedekind for the fruitful discussions on the atmospheric chemistry implications of the study. We acknowledge Prof. Dr. M. H. Schroth and B. Studer for the instrumental support on the ion chromatography analyses and Dr. G. Getzinger for the optimization of the solid phase extraction procedures of the Prairie Pothole samples. We thank Prof. Dr. K. Mopper for the collection of Dismal Swamp water (2014), Dr. V. S. Lin also for the collection of Dismal Swamp water (2016), Dr. C. Chu, C. A. Davis, Dr. E. Janssen and M. Schmitt for the collection of water from Étang de la Gruère, Dr. M. Sander, N. Walpen, Dr. G.

Getzinger and Prof. Dr. M. H. Schroth for the collection of the Storhultsmossen pool water samples, and Prof. Dr. W. Arnold and his group for having provided the surface and porewater samples from the Prairie Pothole wetlands. The authors acknowledge ETH Zurich for funding.

Author contributions: RO, PRE, JT, LHEW and KM designed the experiments. RO and BC performed the irradiation experiments, the IC and UPLC analyses. JT performed the ICP-MS/MS and the HPLC-ICP-MS/MS analyses. RO analyzed the data and wrote the manuscript with contributions from all authors.

Supplementary Materials:

Texts S1-S5

Figures S1-S8

Tables S1-S5